HAL
open science

High Impact Polystyrene/CNT nanocomposites: Application of volume segregation strategy and behavior under extensional deformation

Marjorie Marcourt, Philippe Cassagnau, René Fulchiron, Dimitri Rousseaux, Olivier Lhost, Simon Karam

To cite this version:

Marjorie Marcourt, Philippe Cassagnau, René Fulchiron, Dimitri Rousseaux, Olivier Lhost, et al.. High Impact Polystyrene/CNT nanocomposites: Application of volume segregation strategy and behavior under extensional deformation. Polymer, 2018, 157, pp.156-165. 10.1016/j.polymer.2018.10.032 . hal-02010875

HAL Id: hal-02010875

https://hal.science/hal-02010875

Submitted on 14 Dec 2022

HAL is a multi-disciplinary open access archive for the deposit and dissemination of scientific research documents, whether they are published or not. The documents may come from teaching and research institutions in France or abroad, or from public or private research centers.

L'archive ouverte pluridisciplinaire **HAL**, est destinée au dépôt et à la diffusion de documents scientifiques de niveau recherche, publiés ou non, émanant des établissements d'enseignement et de recherche français ou étrangers, des laboratoires publics ou privés.

High Impact Polystyrene / CNT Nanocomposites: application of volume segregation strategy and behavior under extensional deformation.

Marjorie Marcourt, Philippe Cassagnau, René Fulchiron*,

Univ Lyon, Université Claude Bernard Lyon 1, CNRS UMR 5223, Ingénierie des Matériaux Polymères, F-69622, Villeurbanne Cedex, France

Dimitri Rousseaux, Olivier Lhost, Simon Karam

Total Research and Technology Feluy Zone Industrielle Feluy C 7181 Feluy, Belgium

***Corresponding author : rene.fulchiron@univ-lyon1.fr**

Keywords: Nanocomposites; Extensional Viscoelasticity; Electrical conductivity.

Abstract :

The present work focuses on the analysis of two composites: a pure amorphous Polystyrene and a rubber modified Polystyrene (High Impact Polystyrene), both filled with Carbon Nanotubes (CNT) for generating Conductive Polymer Composites (CPC). Recently, CPC has been obtained with very low filler content following a volume segregation strategy which maintains the filler in one continuous phase. This phenomenon enhances the contacts between fillers and consequently gives birth to conductive composites with ultra-low filler concentration. In this work the two composites are analyzed using a specific set-up that gives the possibility to monitor both electrical conductivity evolution and the elongational stress in the melt state. This set-up allows determining the maximal deformation that nanocomposites can undergo before becoming insulating. In addition, the dynamic of the network evolution that is, its destruction and structuring has been analyzed. When the destruction is predominant, the two composites behave the same. However, we have observed a slight disparity when there is a possible competition between destruction and structuring during extensional deformation. This difference has been accounted to the presence of the nodules that might locally prevent the structuring mechanism during extensional deformation.

A. Introduction

Owing to their good mechanical [1,2], electrical[3], and thermal [4] properties and their specific shape, Carbon Nanotubes (CNTs) are the ideal fillers for the generation of conductive polymer nanocomposites. This specific filler, due to its large aspect ratio, leads to composites with a lower percolation threshold compared to Carbon Black (CB). To push further the boundaries of percolation threshold, a new strategy has emerged. The idea is based on the tailored filler localization in the nanocomposite in order to enhance the formation of the percolated network by confining the fillers. The CNT network architecture design is based on the volume exclusion or on forced segregation.

One strategy is to use immiscible polymer blends in order to force the filler segregation by a privileged affinity between one polymer and the CNTs. The use of immiscible blends for the generation of Conductive Polymer Composites (CPCs) was first investigated by Sumita *et al.* [5,6] with CB. The goal is to generate at least one continuous phase in which the fillers will be located. This volume restriction will enhance the formation of a percolated network. Afterward, this strategy has been investigated in a lot for different kind of fillers [7-15]

Generally, the determination of the filler localization is achieved with only thermodynamic consideration. The minimization of the interfacial energy will drive fillers into the most energetically preferred phase. The localization may be predicted by the calculation of the interfacial energy. Considering a blend made of two polymers P_1 and P_2 and CNT fillers, the wetting parameter ω_{12} can be calculated according to Young's equation for the adjustment of wetting angles on an ideal plane [16].

$$\omega_{12} = \frac{\gamma_{CNT-P2} - \gamma_{CNT-P1}}{\gamma_{P1-P2}}$$

Equation 1

with $\gamma_{i\text{-}j}$ representing the interfacial tension between the components *i* and *j* which are alternatively the filler, the polymer P_1 or the polymer P_2. The value of ω_{12} forecasts the filler localization: if $\omega_{12} > 1$ MWCNT will be in the P_1 matrix, whereas, if $\omega_{12} < -1$ they will be in the P_2 and finally if $-1 < \omega_{12} < 1$, MWCNT will be found at the interface of the different matrices.

The thermodynamic prediction is enough when considering two polymers with truly different polarities and surface energy [3,17-20]. However, to be more accurate, the kinetic aspect must be considered by taking into account the processing conditions, the physical properties of the CNTs, the filler dispersion state and the mixture procedure. For instance, some have observed that the addition of nanofillers can refine and even stabilize the continuous microstructure [21,22]. The best scenario for minimizing the percolation threshold is when the fillers are localized at the interface of the polymer phases. However, this specific case is quite hard to achieve. For instance, Gödel and coworkers have put in the light the impact of the filler shape. Indeed, fillers with a low aspect ratio (such as CB) segregated at the interface of Polycarbonate/SAN blend are more efficient to stabilize the morphology than CNTs [10].

Nevertheless, the generation of composites with a controlled localization of the filler can be achieved and tuned by the functionalization of the filler to control the chemical affinity with a specific phase, by adapting the polarity [23], or grafting of polymer chains [24,25] or by kinetic consideration [26-32].

Leaving apart all experimental conditions, the conductivity of such composites can be tuned by the blend composition (i.e. volume and morphology) of the phase containing the filler. For instance, Xu and coworkers have experienced an increase of five decades in conductivity by varying the blend composition [33]. Only few works dealt with the co-polymers of Polystyrene (PS). For instance, Moldenaers and coworkers [34,35] achieved to gain four decades in conductivity by playing on the molecular weight M_w and the structure of poly(styrene-random/block-methyl methacrylate) for the generation of PαMSAN/PMMA 40/60 filled with MWCNT. In addition, Mclory *et al*. [36] have dispersed MWCNT in High Impact Polystyrene (HIPS) (melt mixing strategy) and obtained a rather large electrical percolation threshold (≈2wt%). By increasing the bead content from 30 to 60 wt% at a constant MWCNTs content of 0.6wt% Shrivastava and coworkers [37] have obtained an increase of 2 decades of the electrical conductivity.

In addition to the increase of the electrical properties, the aggregates form an elastic network within the matrix. This is characterized by the storage modulus that becomes independent of the frequency in the low frequency range ($G' \propto \omega^0; G' = Ge$). In the literature the variation of the equilibrium modulus as a function of the filler concentration has been widely investigated [38-40] and it is well accepted that the value of the storage modulus illustrates the whole response of the local contribution within the network, depending on the network structure and the filler-filler physical connections. More precisely, the filler concentration can be linked to the equilibrium modulus by combining fractal concept for the description of the filler structure and Kantor-Webman model that describes the elasticity of a chain made of particles. The concept of fractal is widely used for composites with filler in the nano to micrometric range [41-45]. Different models have been exposed. Among them, Heinrich and Klüppel have proposed a Cluster-Cluster Aggregation (CCA) model that differs from the others with the assumption that fillers position can fluctuate around a mean value [46-48]. This assumption can be applied to CNTs because these fillers in the nanometer range are highly sensitive to the polymer chains mobility. Heinrich *et al*. have made the assumption that the clusters act as molecular springs with an end-to-end distance ξ, composed of N_B backbone units of length *d*. The backbone can be described as N_B with $d_{f,B}$ a fractal dimension that describes the backbone connectivity. From the expression of the constant force of the cluster backbone, they have obtained an elastic modulus of the cluster backbone and finally from scaling arguments they have obtained the evolution of the whole elastic modulus (considering three-dimensional case) as:

$$G_e \approx G_A \phi^{\frac{3+d_{f,B}}{3-d_f}}$$

Equation 2

where G_A is the elastic modulus of a cluster unit, ϕ is the volume fraction, $d_{f,B} \approx 1.3$ for the smallest fractal dimension of the CCA-cluster backbone and d_f ≈1.8, thereby the exponent $(3 + d_{f,B})/(3 - d_f) \approx 3.6$ [38].

However, the exponents reported in the literature for MWNT dispersed in both thermoplastic and thermoset matrix shows a great discrepancy. For instance, Pötschke *et al*. have obtained 0.2 and 2.5 for MWCNT dispersed in respectively Polyurethane [49] and Polycarbonate [50]. Hobbie and coworkers have observed a power law of 7.1 for MWNT dispersed in Polyisobutylene [51]. In addition, Esteban *et al*. [52] has observed a power law of 1.7 for MWCNT dispersed in unsaturated polyester resin.

This paper aims at studying the volume segregation effect in HIPS filled with CNT composites. The morphology will be compared to a more simple material: a pure PS matrix filled with CNTs. The percolation threshold, the structure of the filler network, the concentration dependence of the equilibrium modulus and the composites behavior under extensional deformation using a specific set-up will be analyzed. A particular attention will be devoted to the dynamic of the filler network structuring and its destruction during extensional tests.

B. Experimental

1) Materials and blends preparation

The CNTs are the NC7000, supplied by Nanocyl a Belgium company. They are characterized by a diameter *d* around 9.5nm and a mean length of 1.5µm. The two matrices used are a PS with a melt flow index of 2.4 and a High Impact Polystyrene (HIPS) with a melt flow index of 2.6 were both supplied by Total. In HIPS, nodules of Polybutadiene (PB) are included to improve the impact strength of the material. The composites are melt mixed using a masterbatches dilution strategy and were supplied by Total as pellets. The specimens were compression molded at 200°C.

2) Morphology analysis

The morphologies have been investigated by Scanning Electron Microscopy (SEM) using a device LSM800 from Zeiss. The detection was ensured owing to in-Lens detector which is located inside the beam focusing lens. The observations have been carried out with a distance between the surface and the final condenser lens (the working distance WD) of around 5mm, an aperture size fixed at 30µm and the accelerating voltage ranging from 10 kV to 20 kV. As the in-Lens detector is very sensitive to surface roughness, the sample surface has been cut with a diamond knife to prevent any roughness and promote the contrast between electrically conductor filler and insulating matrix. For the HIPS composite, the sample surface was firstly immerged in $Os0_4$ solution for at least four days in order to increase the phase contrast and make easier the specimen preparation by rigidifying the PB nodules. The observation technique will not be detailed in the paper, however the reader can refer to studies on this method [53,54]. In addition, Transmission Electron Microscopy observations have been carried out in order to complete the morphology characterization. Thin films have been cut at room temperature after the same specimen preparation as for the SEM characterization.

3) Conductivity measurement

Electrical properties analysis has been conducted on compression molded samples that have been additionally submitted to a quiescent treatment at 200°C for about 20 min. This supplementary thermal treatment enables the filler network to recover an equilibrium state in which most of the CNTs take part to the electrical conduction. Indeed, just after the compression molding, this state is not obtained. A colloidal silver paste was applied on the surface sample to ensure a good contact between the electrodes and the specimen surface. Owing to a Keithley 237 power supply, a 10 volt Direct Current (DC) is delivered and the current passing through the sample is measured. The volume conductivity is then deduced using the specimen geometry as:

$$\sigma = \frac{L.I}{S.U}$$

Equation 3

with U the applied voltage, I the measured current, L and S respectively the specimen length and section.

4) Rheological measurements

Dynamic measurements were performed using an Ares rheometer (TA Instruments) equipped with parallel plates of 25 mm diameter under nitrogen atmosphere. The pure matrices where analyzed in the linear viscoelastic domain using the strain-controlled rheometer at different temperatures. Then following the time-temperature superposition principle, master curves have been built for a reference temperature of 200°C. The master curves were then described by a classical Maxwell N modes model [55]:

$$G'(\omega) = \sum_{i=1}^{N} \frac{G_i \omega^2 \lambda_i^2}{1 + \omega^2 \lambda_i^2}$$

Equation 4

$$G''(\omega) = \sum_{i=1}^{N} \frac{G_i \omega \lambda}{1 + \omega^2 \lambda_i^2}$$

Equation 5

where G_i is the modulus contribution corresponding to the relaxation time λ_i. For the fitting, the λ_i were fixed over the range of time constants corresponding to the reverse of the experimental frequency range. Using an iterative non-linear least square regression algorithm applied to the relative difference between calculated and experimental complex moduli $G^*(\omega)$, the G_i contributions were deduced. The number of modes was fixed as the best compromise between the fitting quality and physically adequate (non-negative) values of the G_i. The frequency range for the HIPs matrix is chosen in order to characterize the relaxation mechanism attributed to the PS phase (frequency range > 0.1 rad/s). In Figure 1 the master curves are displayed fitted by a 5 modes Maxwell model for the pure PS matrix and by a 6 modes Maxwell model for the HIPS matrix.

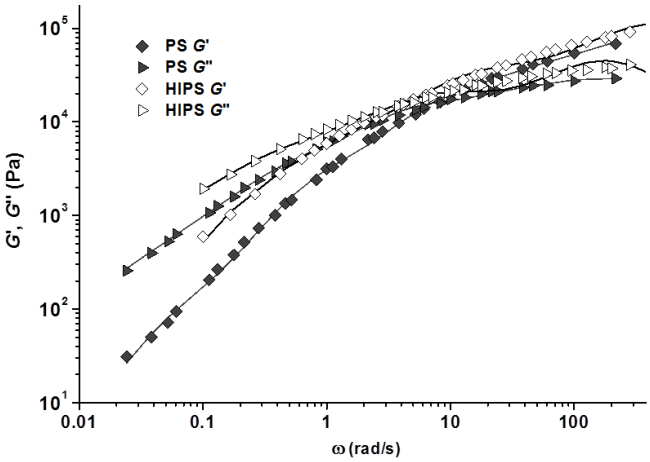

Figure 1 : Master curve of PS (filled symbols) and HIPS (open symbols) matrices built for a reference temperature of 200°C. Symbols: E xperimental data *G'* and *G"*, Solid lines: Discrete Maxwell model.

The weight average relaxation time λ_w can be calculated from the λ_i and G_i parameters by:

$$\lambda_w = \frac{\sum_{i=1}^{n} G_i \lambda_i^2}{\sum_{i=1}^{n} G_i \lambda_i} = \eta_0 J_e^0$$

Equation 6

The build of the master curve gives access to the shift factors a_T, that follow the William Landel Ferry equation [56, 57]. Table 1 displays the weight average relaxation times for the two matrices determined from the master curves at a reference temperature of 200°C and calculated at different temperatures using the appropriate shift factors also given in Table 1.

Table 1 : Shift factors a_T and weight average relaxation times for the two matrices calculated for different temperatures

T°C	a_T (PS)	λ_w for the pure PS matrix (s)	a_T *(HIPS)*	λ_w of the PS in the HIPS matrix(s)
210	0.506	2.1	0.553	1.7
200	1	4.2	1	3.2
180	6.24	26	4.49	14
160	115	483	38.6	124

In addition, the viscoelastic behavior of the PS-MWCNT and HIPS-MWCNT filled with 0.15; 0.3; 0.6; 0.8; 1; 1.25; 1.5; 2; 3 wt% were analyzed at 200°C at a strain fixed to 1% chosen in the linear viscoelasticity domain. In order to control the aggregation state of the composites, the samples were first annealed for 20 min before the dynamic measurement. In an early study [58], we have shown that the filler concentration does not impact the dynamic of the polymer chains. In this work, the weight average relaxation time of the pure matrix will be used to calculate the Weissenberg number for the different extensional experiments. Indeed, we consider that the polymer molecular mobility remains unaffected by the CNT network.

5) Extensional deformation combined with conductivity measurement

Extensional experiments were carried out with a commercialized Extensional Viscosity Fixture EVF (TA instruments) mounted on the ARES rheometer (TA instruments). The set-up was modified in order to measure the specimen conductivity during the extensional test. This specific set-up has already been detailed in an earlier work [58].

C. Results and discussion

1) Morphology

The different morphologies of the composites will be first analyzed. Figure 2 shows a TEM micrograph of the HIPS/MWCNT. With interfacial energy from the literature, the wetting coefficient $\omega_{PS\text{-}PB}$ can be calculated and it is found equal to 2 at 200°C [59,60]. By considering the thermodynamic prediction ($\omega_{PS\text{-}PB}$>1), the MWCNTs have a better affinity with PS than PB.

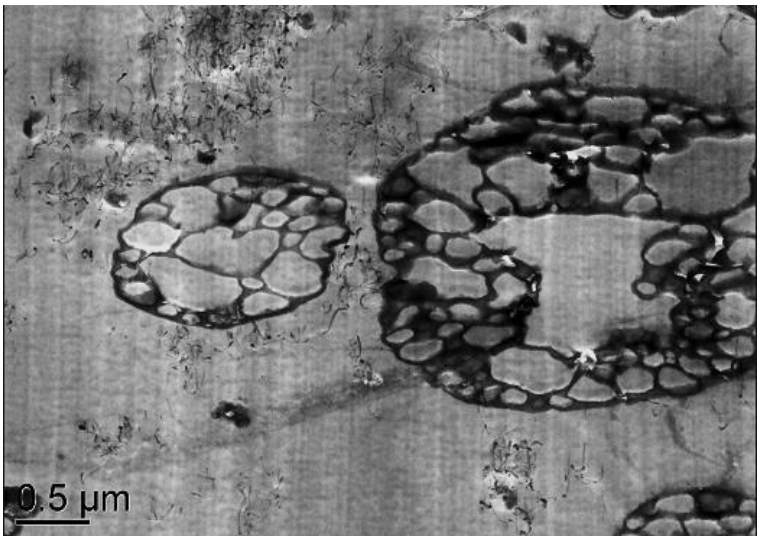

Figure 2 : TEM micrograph of HIPS filled with 0.82 vol% CNT

In this work, the CNTs were first melt mixed in a PS matrix for the generation of a highly filled masterbatch and then diluted with rubber-modified PS to obtain composites with a tailored filler concentration. CNTs are not expected to be found in the PS phase inside the PB nodules, because they should have to pass through the PB envelope. This is shown by the TEM micrographs where the CNTs are located in the PS phase outside the nodules.

Figure 3 shows two Scanning Electron Microscopy (SEM) micrographs of both composites filled with ~0.8 vol% of MWCNT. The observation is carried out with SEM with the in-lens detector. This detector gives the possibility to the observation of the CNTs thanks to enhanced contrast between the fillers and the matrix [53,54]. The bright dots are CNTs. The dark phase is the insulating PS matrix and the grey scaled phases are the PB nodules functionalized with OsO_4.

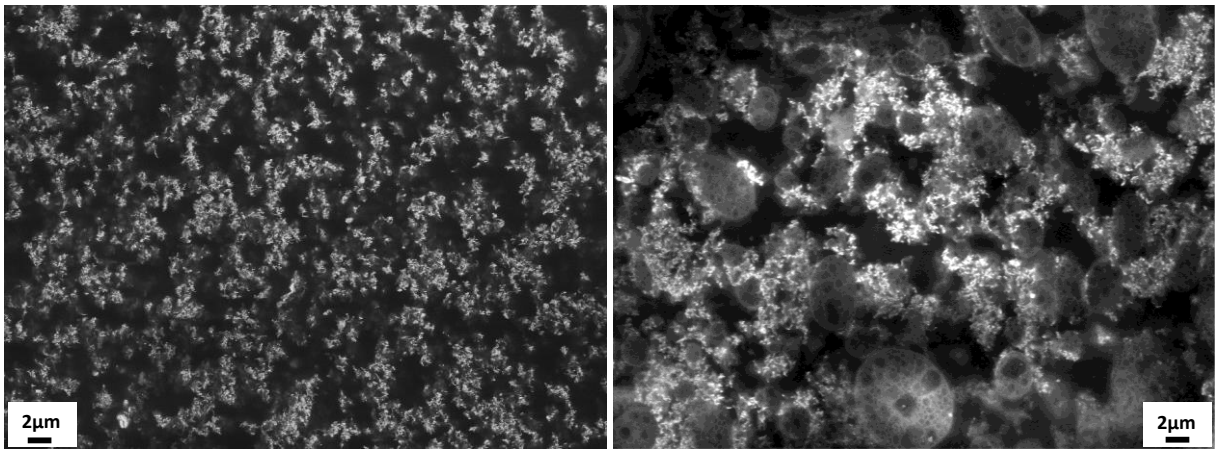

Figure 3 SEM micrographs of PS filled with 0.79 vol% MWCNT (left) and HIPS filled with 0.82 vol% MWCNT (right), magnification = x2000, WD 5mm 20kV and in-lens detector.

In the PS matrix, the CNTs form a well percolated network of aggregates homogeneously distributed (Figure 3a). Figure 3b shows that in the HIPS matrix; the aggregates make a network in the PS rich phase around the nodules. The aggregates seem to be larger in the HIPS/MWCNT composites than in the PS/MWCNT composite. Due to not enough contrast within micrographs this assumption could not be confirmed by image analysis. In addition, the volume of the PB nodules in the HIPS has been estimated to 40 vol% by TEM analysis.

2) Effect of the nodules on the electrical conductivity

The conductivity in Conductive Polymer Composites arises when the fillers form a percolated network within the material [61,62]. Classical percolation theory has been applied in order to determine the percolation threshold and the exponent for the two composites.

$$\sigma = \sigma_0(\phi - \phi_c)^t$$

Equation 7

First of all, one must mention that during the melt mixing the CNT length can be reduced. The length distribution of the CNT after melt processing has been determined in TEM analysis on samples after the matrix has been removed with appropriate solvent. This analysis has only been carried out on the HIPS composite; as the processing conditions are quite comparable one can make the assumption that the length distribution is similar for the two matrices.

Fillers with aspect ratio in the range of 100 can theoretically generate composites with a percolation threshold a few lower than 0.1 vol% [63]. From the measured conductivities, the percolation law parameters, σ_0 and t, were determined from simple linear regressions on the logarithmic form of Equation 7 by adjusting the percolation threshold ϕ_c (maximizing the determination coefficient r^2 of the linear regressions). The obtained exponent is 1.74 with a percolation threshold at 0.33 vol% of CNT for the PS/CNT composite and respectively 2.24 and 0.16 vol% for the HIPS/MWCNT composite. Hence, the two composites lead to slightly larger percolation thresholds than expected. The exponents illustrate the formation of a 3D network according to the percolation theory. As expected, due to the segregation of the fillers [5-7,9] the HIPS matrix generates composites with a lower percolation threshold than the PS matrix. In order to explain the

difference between the two composites, the effective concentration of the CNT in the PS phase outside the nodules has been calculated with Equation 8:

$$\phi\ (vol\%) = \frac{V_{CNT}}{V_{CNT} + V_{PS}} \times 100$$

Equation 8

where V_{CNT} is the volume occupied by CNT aggregates and V_{PS} is the volume occupied by PS. Taking into account the PS phase accessible to the fillers gives the possibility to explain the different percolation thresholds obtained. Figure 4 shows the conductivity evolution as a function of the nominal CNT concentration for both PS and HIPS matrices. The corresponding percolations laws are also plotted. Moreover, the conductivity variation for the HIPS matrix is also plotted versus the CNT volume fraction in the accessible PS phase calculated with Equation 8. The conductivity evolutions as a function of this corrected concentration for the two different matrices superimpose very well showing the efficiency of the volume segregation resulting from the presence of PB nodules.

Hence, taking into account the effective volume concentration of the fillers in the PS phase for the HIPS composite, the matrices lead to similar percolation threshold. The nodules are randomly dispersed in the continuous PS phase. Thus, the conductivity of the material is preserved. Last, but not the least, the presence of the nodules which occupy around 40 % of the total volume gives the possibility to decrease the global CNT weight concentration of nearly 50 %. It must be mentioned that, everywhere in the following of this work, the considered volume concentration of CNT will be the corrected concentration in the PS phase considering the restricted volume. However, it can be noticed in Figure 4, that the HIPS conductivity (after correction) may appear slightly lower than the PS composite conductivity. This is certainly due to the effective section of electrical pattern which are smaller in the HIPS composite than in the pure PS.

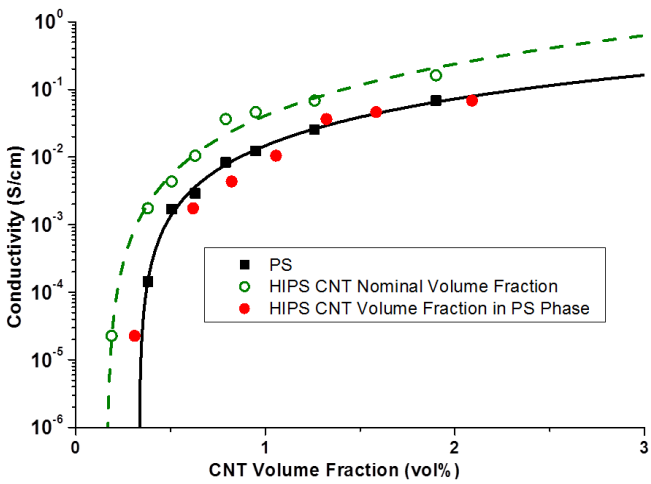

Figure 4 : Evolution of the conductivity as a function of the volume fraction of MWCNT. Empty circles and filled squares: raw data. Solid and dashed lines: percolation laws respectively for the PS and HIPS matrices. Filled circles: conductivity measured in the HIPS matrix and plotted versus the volume fraction of CNT in PS Phase (see Eq. 8). .

3) Effect of the volume segregation on the filler network structure

The percolation theory applied to composites made of insulating matrix filled with electrically conductor particles gives the possibility to characterize the insulating/conductor transition. However, this concept does not give further details on the network structure. That is why, in addition to volume conductivity measurements, dynamic rheology measurements have been carried out on both composites in order to investigate the network formation and its evolution as a function of the CNTs concentration. It must be pointed out that attention has been paid on the modulus measurement since CNTs networks are very sensitive to the experimental conditions and especially to the melt history [64,65]. The aggregation state must be controlled in order to characterize a well-structured network. That is why in this work, the storage modulus has been measured after an annealing treatment of around 20 min for the two composites. The experimental curves of *G'* as a function of the angular frequency are shown for different CNTs concentrations in Figure 5 for the PS composites and in Figure 6 for the HIPS composites.

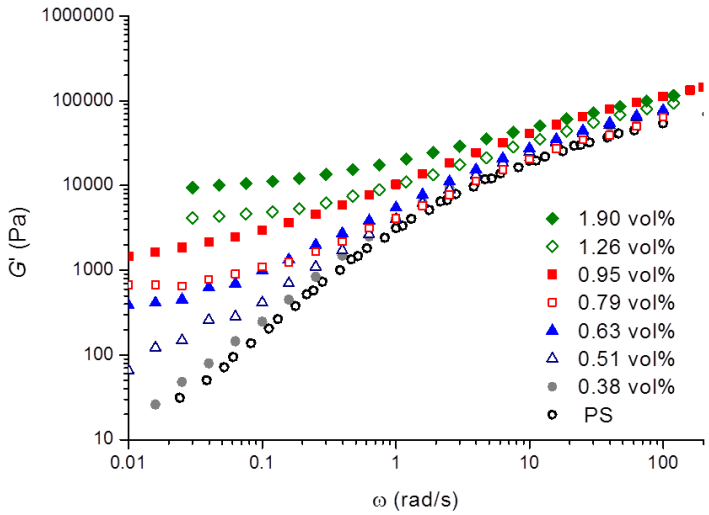

Figure 5 : Storage moduli versus angular frequency at 200°C for PS composites.

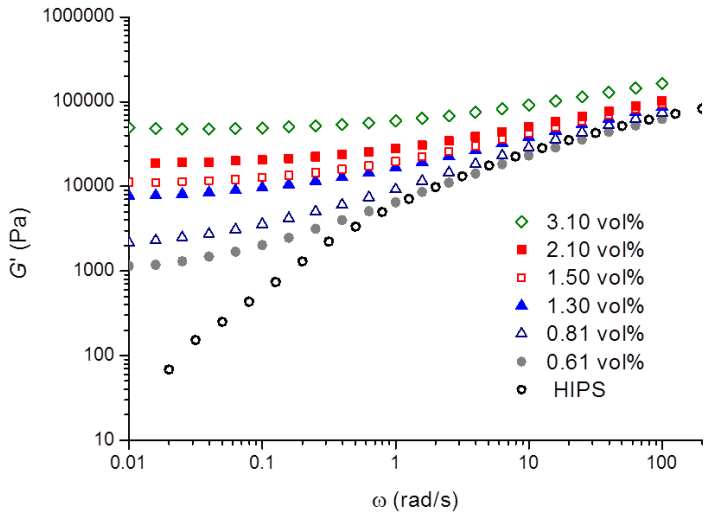

Figure 6 : Storage moduli versus angular frequency at 200°C for HIPS composites (indicated volume concentrations are concentrations in the PS phase).

Like the evolution of the conductivity, the increase of the equilibrium storage modulus G_e that is, the plateau modulus appearing in the low frequency region for percolated structures, can be described with a percolation law:

$$G_e \approx G_0(\phi - \phi_c)^t$$

Equation 9

The determination of the percolation threshold ϕ_c has been achieved again by the maximization of the determination coefficient r^2 of the logarithmic form of Equation 9, giving the other parameters G_0 and t at the same time. A value of ϕ_c equal to 0.22% was obtained for the PS matrix and of 0.24% for the HIPS matrix. These values are very close to each other consistently with the consideration of the CNT fraction only in the PS phase for the HIPS as it was shown for the conductivity. Nevertheless, it must be conceded that this percolation threshold is slightly lower than this obtained for the conductivity with the PS matrix (0.33%) but it must be kept in mind that the comparison between percolation thresholds coming from mechanical and electrical techniques can be somewhat questionable. Particularly, in the present case, the matrix (PS or HIPS) is in the melt state for the rheological measurements while it was solidified for the conductivity.

Figure 7 shows the evolution of the equilibrium modulus as a function of the filler concentration in the PS. The equilibrium moduli of the HIPS composites are larger than these of the PS composites, evidently due to the presence of the PB nodules which leads to a higher modulus of the sole matrix itself. The curves given by the percolation laws are also displayed in Figure 7. For the composites with the PS matrix, the obtained exponent is 2.76 close to the value of 2.5 reported by Pötschke et al. for CNT in polycarbonate [50]. However, the HIPS composites materials exhibit a lower exponent of 1.84. This difference compared to the pure PS matrix may be due to a different structure of the network in the HIPS composites.

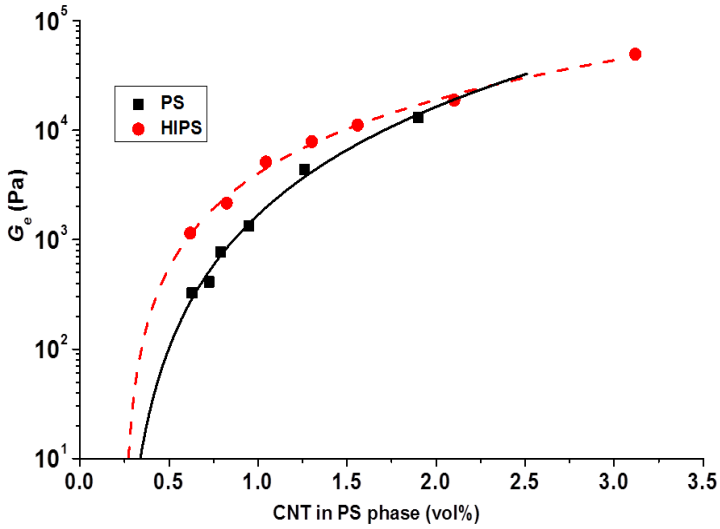

Figure 7 : Variation of the equilibrium modulus as a function of the CNT volume fraction in PS continuous phase. Symbols: Experimental data. Lines: Percolation laws.

4) Analysis of the filler network under extensional deformation

The extensional viscosity of the materials have been measured at different temperatures in the range of 140°C to 210°C and different elongation rates between 0.01 s^{-1} to 0.1 s^{-1}. In Figure 8 is plotted the ratio between the composites extensional viscosity at 180°C and 0.1 s^{-1} and the zero

shear viscosity of the unfilled material. For concentrations up to 1 vol% the obtained ratio is around 3 as expected for the classical Trouton's ratio. Thus, the presence of a percolated network does not influence the extensional viscosity. However, for the HIPS based composites at filler volume concentrations above 1 vol%, a large deviation is observed, whereas this deviation is not observed for the PS based composites. This deviation can be accounted for the segregation that enhances the formation of connections between the aggregates in the HIPS.

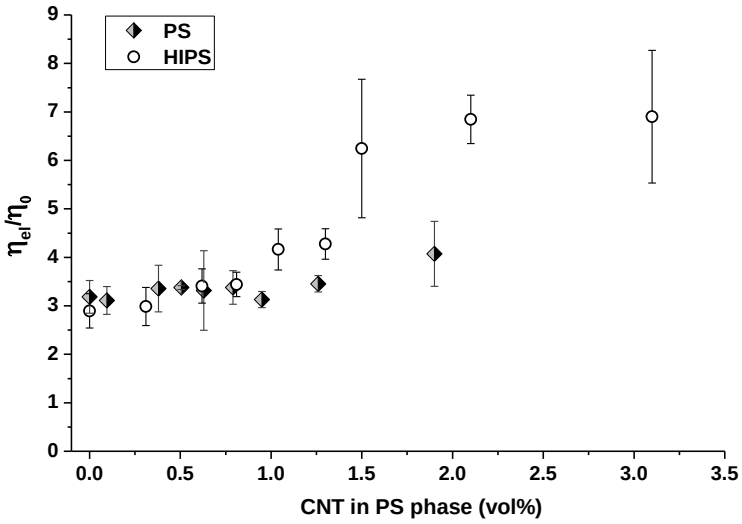

Figure 8 : Ratio between extensional viscosity at 0.1 s^{-1} of the composites and the shear viscosity of the matrices at 180°C

It has been observed that the deviation from the Trouton's ratio of 3 occurs at a lower CNT content when using CNT with larger aspect ratio or highly filled suspension [68,69]. In addition, the analysis of the linear viscoelastic behavior has shown that the network strength is higher in the HIPS than in the PS. This denser filler network has a crucial impact on the material flow ability. Concomitantly, with this large deviation, a smaller strain-at-break is observed for the HIPS based composites. In the literature, the PS strain-at-break is larger than for HIPS or even blend of PS and HIPS matrices [70]. Even if the filler content is quite low the generated interface volume is very large. The polymer chains embedded within the filler network do not have exactly the same behavior than in pure matrix. Their mobility is strongly reduces and the break appears at lower strains.

At large filler concentration, the flow ability of the HIPS composite is dramatically impacted. From a pragmatic point of view, the use of nanofillers with large aspect ratio is motivated by their potential in the generation of conductive composites with low amount of fillers. Nevertheless, the small effect of the CNT on the measured extensional stress is not enough to provide valuable information on the filler network evolutions.

The composites have been analyzed using a specific set-up of combined conductivity and extensional viscosity measurements. This set-up gives the possibility to measure the electrical conductivity variation of the melt specimen which experiences an extensional deformation at a constant strain rate. Figure 9 shows the conductivity variation of two composites filled with about 0.8 vol% of CNT in the PS phase at 160°C and an extensional rate fixed at 0.01 s^{-1}. The slight concentration difference between the two composites and the fact that at a Hencky deformation ε equal to 0, the two specimens are not at their equilibrium state have no strong impact on the following results.

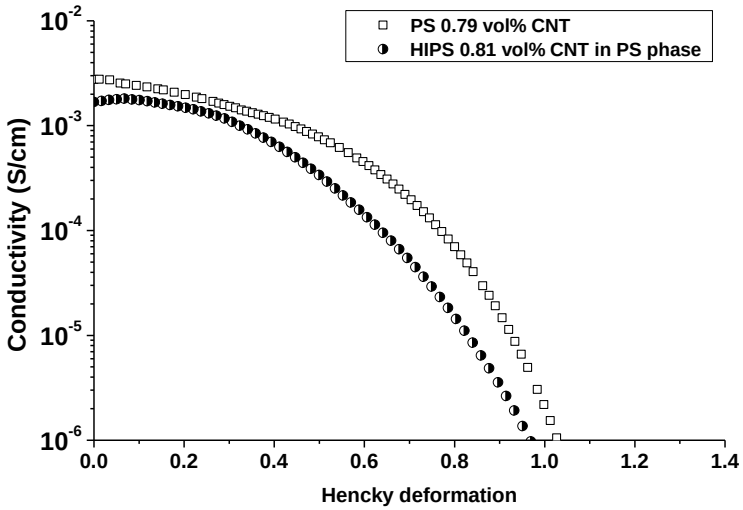

Figure 9 : Conductivity evolution under extensional deformation at 180°C for an extensional rate of 0.01 s^{-1}

For the two specimens, the conductivity decreases during the extensional experiment. As explained in our previous work [58], the conductivity decrease results from the progressive destruction of the filler network during the extensional test. The connections between the aggregates break due to the deformation of the sample. The two curves follow the same variation except that the HIPS composite shows a slightly faster decrease. Notwithstanding, this small difference is not enough significant to conclude.

The morphology of the two specimens after a Hencky deformation of 1 has been characterized. The two SEM micrographs are presented in Figure 10 where the white arrows illustrate the deformation direction. The structure of the PS composite (see Figure 10a) is made of aggregates stretched and oriented in the deformation direction. However; the structure of the HIPS morphology (see Figure 10b) is somewhat more difficult to characterize due to the presence of the PB nodules. First, the aggregates are stretched like in the pure PS matrix, but their orientation is less pronounced. Moreover, due to the PB nodules, the extensional rate is not homogeneous in the material and this can locally orient the aggregates in different directions than the whole deformation direction. In the following, the recovery mechanism and the competition between structuring and destruction mechanisms during the extensional deformation will be investigated more precisely.

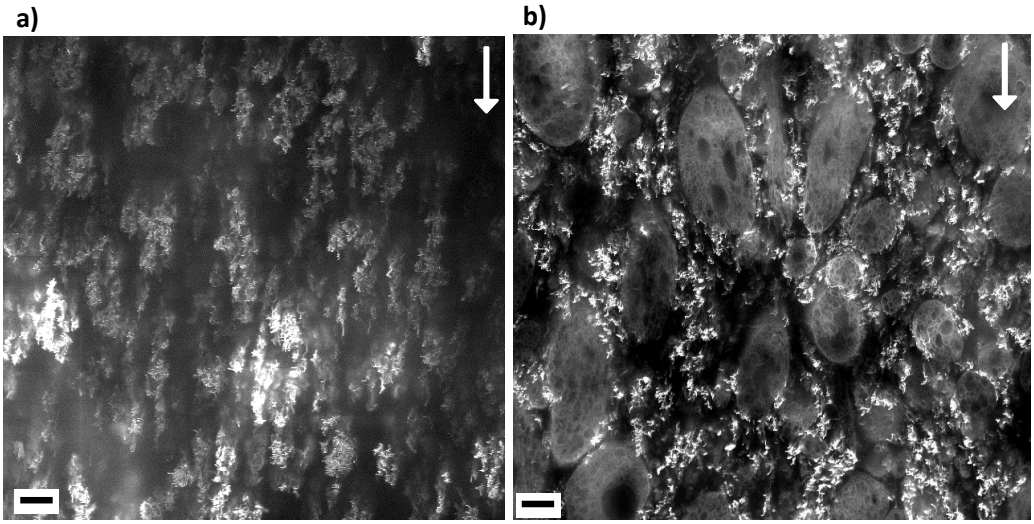

Figure 10 : SEM micrographs of the two composites after a Hencky deformation of 1 at 160°C and 0.01 s^{-1} a) PS filled with 0.79 vol% CNT, b) HIPS filled with 0.82 vol% CNT in the PS phase and the conductivity is around 8.10^{-5} S/cm for the two specimens. The scale bar is 2µm.

The conductivity recovery is a phenomenon largely addressed in the literature [71-75]. In our previous work carried out on PS filled with MWCNTs [58], we have shown that the polymer dynamics plays a major role in this mechanism. Indeed, the polymer chains govern the recovery mechanism as it gives sufficient mobility for isolated CNT or highly disentangled bundle of CNTs for the formation and reinforcement of the network. Here, the conductivity recovery has been analyzed for the HIPS composite following the same methodology. Specimens filled with about 0.80 vol% have been deformed in order to investigate the following conductivity recovery under quiescent conditions. This experience has been carried out at different temperatures. Like for the PS matrix composites [58], the conductivity recovery of the HIPS/CNT material fulfills a time-temperature superposition principle. A master curve of the conductivity recovery can be built and one obtains Williams Landel Ferry coefficients close to those obtained from rheological measurements (when using the same reference temperature). Figure 11 displays WLF plots of the a_T shift factors obtained respectively from the dynamic rheology of the pure matrices and from conductivity recovery experiments of both matrices filled with about 0.8 vol%. The reference temperature is 180°C. For the PS composites, the data from the dynamic rheology and conductivity recovery are very close. However, for the HIPS composite a slight difference can be observed between the a_T from the conductivity recovery and those from the dynamic rheology at high temperatures. The possible explanation of this result is that the shift factors obtained from rheology can be blurred because of the presence of the PB nodules which bring some uncertainty in the build of the master curve. Conversely, for the conductivity measurements, the PB nodules do not act in the CNT mobility. Thus, the network structuring is due to the mobility given by the polymer chains. Figure 12 shows the conductivity recovery of the two composites after a Hencky deformation of 1 at 170°C and at 0.01 s^{-1}. The recovery of the two composites superimposes very well. The same results have been observed at higher and lower temperatures (not shown here).

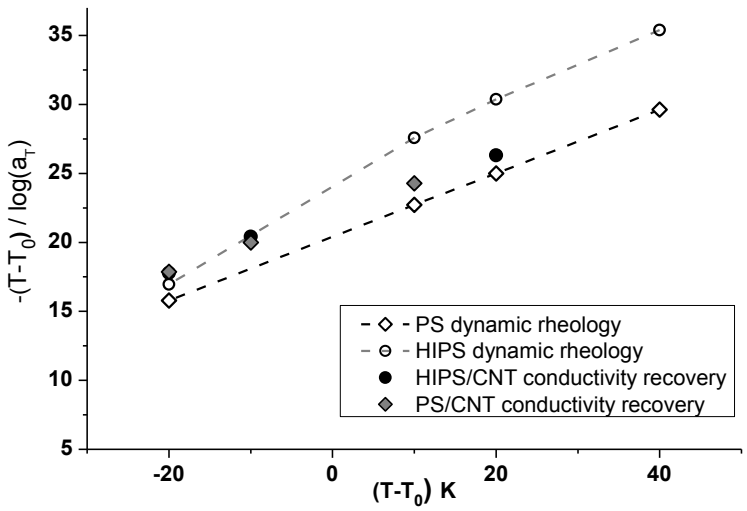

Figure 11 : WLF plot for the a_T shift factor from the build of the master curve of the pure matrices and from the build of the master curve of conductivity recovery. The reference temperature (T_0) is 180°C

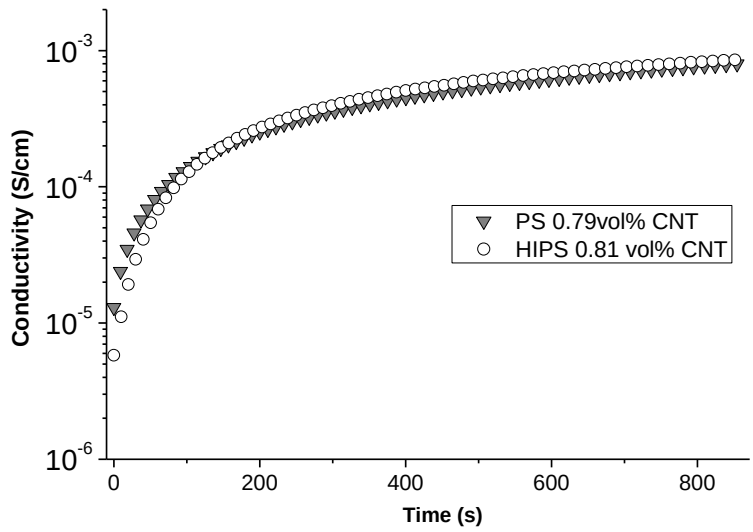

Figure 12 : Conductivity recovery under quiescent condition at 170°C of PS filled 0.79 vol% CNT and HIPS filled with 0.82 vol% CNT after a Hencky deformation of 1 at 170°C and 0.01 s^{-1}

The filler reinforcement is driven by the same mechanism for the two composites. Disentangled and isolated CNT can diffuse and the attractive filler-filler interaction forces trigger the generation of inter-particles connections.

Under extensional deformation, a competition between destruction and restructuring of the network can occur. The use of the Weissenberg number ($\lambda_w \dot{\varepsilon}$) is useful for the determination of which mechanism is predominant. The contribution of the polymer chain mobility is taken into account thanks to the use of the weight average relaxation time of the pure matrix. Figure 13 illustrates the conductivity variations for the two composites under different experimental conditions that cover a wide range of W_i. It can be pointed out that they show different conductivity values at the beginning of the extensional test. This is due to the fact that the specimens are not fully aggregated and depending on the working temperature, they will tend to reach their equilibrium state (i.e. state where all the CNTs take part to the conductivity) with more or less rapidity.

At large W_i, all the measured conductivity curves merge to the same one. It is worth noting that the two materials exhibit the same limiting deformation (ε=1) before becoming insulating (under 10^{-6} S/cm). Under those conditions, the relaxation mechanisms are too slow compared to the extensional rate. By changing the experimental conditions (playing on temperature and on extensional rate), the W_i can be reduced. In this specific case, a competition between restructuring and destruction can be theoretically observed and Figure 13 shows that the specimens can undergo larger deformation before becoming insulating. This shift to larger deformation observed for the two composites illustrates this competition.

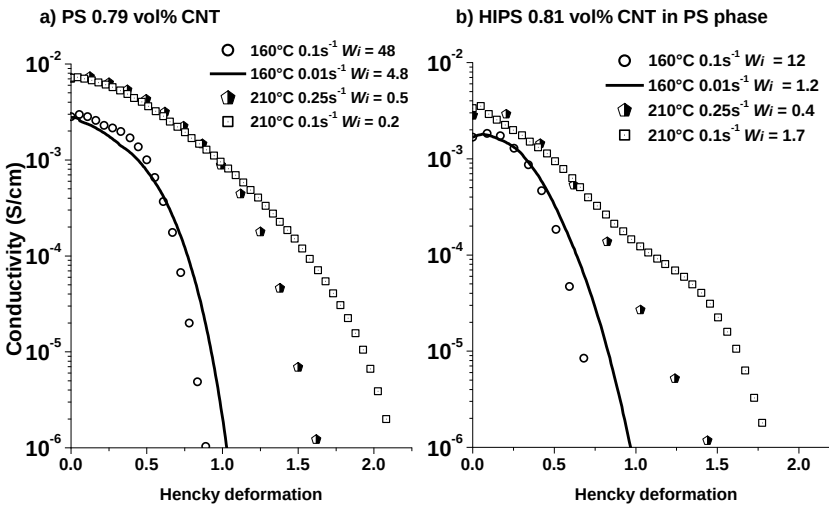

Figure 13 : Conductivity variation for PS filled with 0.79 vol% CNT (a) and HIPS filled with 0.82 vol% CNT (b) under extensional conditions that lead to large and low W_i for the two composites.

In addition, a large range of CNT concentrations have been analyzed. From all the conductivity measurements (not shown here), a specific value of the strain ε_σ was noted. This is the strain for which the sample conductivity dropped to the arbitrarily chosen value of 10^{-6} S/cm. In Figure 14 and Figure 15, this strain is plotted as a function of the filler volume fraction for different extensional conditions that cover low and large W_i values. For the HIPS materials, only the results for specimens with filler concentrations lower than 2.1 vol% have been plotted. Indeed, the specimens filled with larger CNT concentrations were broken very early, that is, for deformations where the conductivity was still high.

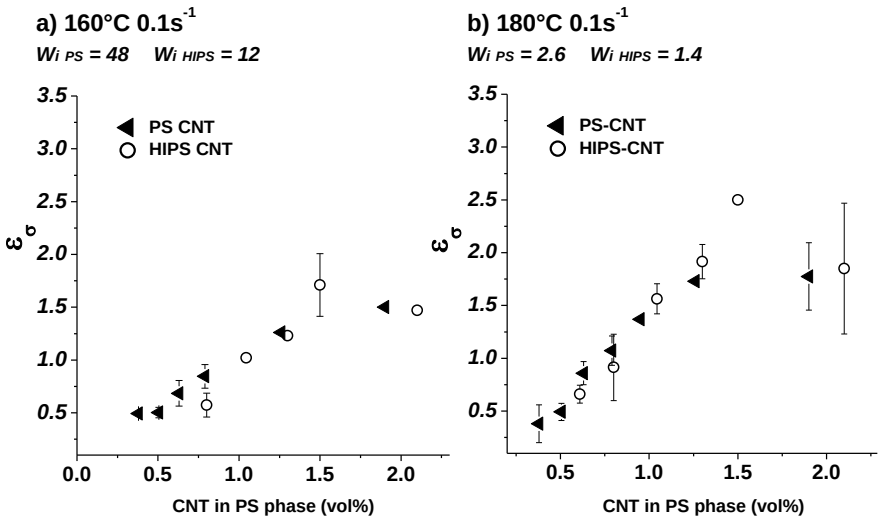

Figure 14 : Evolution of the Hencky strain value when the composites conductivity reaches 10^{-6} S/cm as a function of the filler volume fraction for the two types of matrix for specimen under extensional rate fixed at 0.1 s^{-1} at 160°C a) and at 180°C b)

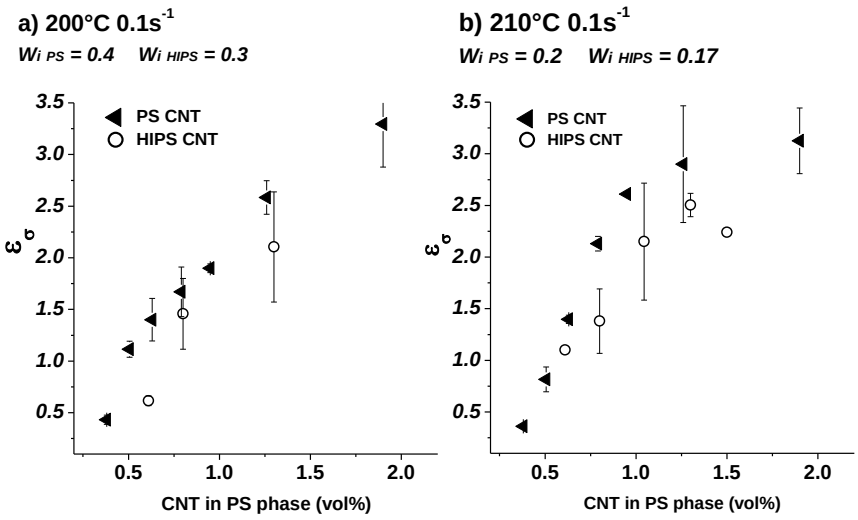

Figure 15 Evolution of the Hencky strain value when the composites conductivity reaches 10^{-6} S/cm as a function of the filler volume fraction for the two types of matrix for specimen under extensional rate fixed at 0.1 s^{-1} at 200°C a) and at 210°C b)

At low temperature, composites based on both matrices present close conductivity variations and the obtained ε_σ superimposed remarkably. However, with the increase of the temperature, the composites with the PS matrix show very slightly larger ε_σ than with the HIPS matrix. Even if λ_w is larger for the pure PS than for the PS in the HIPS matrix (see Table 1), the restructuring phenomena appears more pronounced in the pure PS matrix.

The presence of the nodules and the difference in the aggregates size in the HIPS matrix can influence the network destruction under extensional deformation. Indeed, the deformation rate is not really homogeneous within the sample. Because of the nodules which are less deformed, the deformation rate is larger in some locations of the PS phase. In addition, the presence of the nodules might strongly prevent the formation of connections between aggregates, especially in the deformation direction and consequently, enhances the destruction of the network. Finally, the difference in the filler dispersion state must be kept in mind as only isolated CNTs and disentangled

group of CNTs can acquire sufficient mobility of the matrix. The concentration of this population may be different for the two matrices and may impact the restructuring mechanisms.

D. Conclusion

In this work, two polymer matrices: a pure PS and a rubber-modified PS filled with Carbon Nanotubes have been analyzed in order to put in the light the influence of the restricted volume for the fillers. Indeed, it has been observed that the forces segregation of the filler in the PS continuous phase of the HIPS leads to the achievement of composites with a very lower percolation threshold. Indeed, the HIPS material which contains about 40 volume percent of nodules gives the possibility to decrease by a factor of about 2 the weight fraction of CNTs, while preserving the same conductivity compared to the pure PS matrix. The resulting elastic networks in the two composites are slightly different and this has been attributed to the difference in the dispersion state and more precisely the difference in the size and density of agglomerates that constitute the filler network.

The dynamics of the structuring and destruction of the filler network have been investigated in quiescent conditions and under extensional deformation. Like in the PS/CNT materials, the polymer dynamics in the rubber-modified matrix governs the structuring mechanism.
The competition between structuring and destruction of the network can be weighted thanks to the Weissenberg number defined as the product of the deformation rate and the weight average relaxation time of the matrix. When the restructuring is negligible during the deformation, the two composites have the same limiting deformation before becoming electrically insulating. However, at low W_i, when the restructuring mechanism can compete with the destruction induced by the deformation, the PS/CNT composite shows larger limiting deformation than the rubber-modified composite. Indeed, the restructuring phenomenon is limited for the HIPS/CNT specimens, even if the relaxation time is lower. This has been attributed to the presence of the nodules that can prevent locally the formation of connections between aggregates and induces non homogeneous deformation rate within the specimen.

In addition, a strong deviation from the Trouton's ratio of 3 combined with small strain at break has been observed for the HIPS/CNT specimens when the filler concentration is larger than 1. %. The amount of CNTs impacts the polymer chains mobility and consequently decreases the material properties.

Acknowledgments

This work was funded by the ANRT and Total. The authors kindly thank engineers P. Alcouffe, X. Jaurand and C. Cuccuzzela for significantly help in Scanning Electronic Imaging technics, doctor G. Seytre and technician L. Cavetier for helping setting-up the home made EVF system and engineer and laboratory technician Eddi Scandino for the generation of the different composites.

References

[1] B. G. Demczyk, Y. M. Wang, J. Cumings, M. Hetamn, W. Han, A. Zettl, R. O. Ritchie, Direct mechanical measurement of the tensile strength and elastic modulus of multiwalled carbon nanotubes, Mater. Sci. Eng. A 334 (2002) 173-178.

[2] D. A. Walters, L.M Ericson, M.J. Casavant, J. Liu, D. T. Colbert, K.A. Smith, R. E. Smalley, Elastic strain of freely suspended single-wall carbon nanotube ropes, Appl. Phys. Lett. 74 (1999) 3803-3805.

[3] Z. Yao, C.L. Kane, C. Dekker, High-field electrical transport in single-wall carbon nanotubes, Phys. Rev. Lett. 84 (2000) 2941.

[4] S. Berber, Y.-K Kwon, D. Tománek, Unusually high thermal conductivity of carbon nanotubes, Phys. Rev. Lett. 84 (2000) 4613–4616.

[5] M. Sumita, K. Sakata, S. Asai, K. Miyasaka, H. Nakagawa, Dispersion of fillers and the electrical conductivity of polymer blends filled with carbon black. Polym. Bull. 25 (1991) 265-271.

[6] M. Sumita, K. Sakata, Y. Hayakawa, S. Asai, K. Miyasaka, M. Tanemura, Double percolation effect on the electrical conductivity of conductive particles filled polymer blends, Colloid Polym. Sci. 270 (1992) 134-139.

[7] A. Gödel, G. Kasaliwal, P. Pötschke, Selective localization and migration of multiwalled carbon nanotubes in blends of polycarbonate and poly(styrene-acrylonitrile), Macromol. Rapid Commun 30 (2009) 423-429.

[8] T. Périé, A. C. Brosse, S. Tencé-Girault, L. Leibler, Co-continuous nanostructured nanocomposites by reactive blending of carbon nanotube masterbatches, Polymer 53 (2012) 984-992.

[9] W. Thongruang, C. M. Balik, R. J. Spontak, Volume-exclusion effects in polyethylene blends filled with carbon black, graphite, or carbon fiber, J. Polym. Sci. Pol. Phys. 40 (2002) 1013–1025

[10] H. M. Warth, Mechanical properties and electrical conductivity of carbon-nanotube filled polyamide-6 and its blends with acrylonitrile/butadiene/styrene, Polymer 45 (2004) 739–748.

[11] P. Pötschke, A. R. Bhattacharyya, A. Janke, Morphology and electrical resistivity of melt mixed blends of polyethylene and carbon nanotube filled polycarbonate, Polymer 44 (2003) 8061–8069.

[12] A. Göldel, A. Marmur, G. R. Kasaliwal, P. Pötschke, G. Heinrich, Shape-Dependent Localization of Carbon Nanotubes and Carbon Black in an Immiscible Polymer Blend during Melt Mixing. Macromolecules 44 (2011) 6094–6102.

[13] P. Pötschke, S. Pegel, M. Claes, D. Bonduel, A novel strategy to incorporate carbon nanotubes into thermoplastic matrices, Macromol. Rapid Commun. 29 (2008) 244–251.

[14] M. Wu, L. L. J. Shaw, On the improved properties of injection-molded, carbon nanotube-filled PET/PVDF blends. J. Power Sources 136 (2004) 37–44.

[15] P. Pötschke, A. R. Bhattacharyya, A. Janke, Morphology and electrical resistivity of melt mixed blends of polyethylene and carbon nanotube filled polycarbonate, Polymer 44 (2003) 8061–8069.

[16] T. Young, Philosophical Transactions of the Royal Society of London Works, edited by Peacock, 1805 Vol. 95, p 432.

[17] A. C. Baudouin, J. Devaux, C. Bailly, Localization of carbon nanotubes at the interface in blends of polyamide and ethylene-acrylate copoly-mer, Polymer 51 (2010) 1341–1354.

[18] A. Göldel, A. Marmur, G. R. Kasaliwal, P. Pötschke, G. Heinrich, Shape-dependent localization of carbon nanotubes and carbon black inan immiscible polymer blend during melt mixing, Macromolecules 44 (2011) 6094–6102.

[19] A. Göldel, G. Kasaliwal, P. Pötschke, Selective localization andmigration of multiwalled carbon nanotubes in blends of polycarbo-nate and poly(styrene-acrylonitrile). Macromol Rapid Commun. 30 (2009) 423–429.

[20] L. Zhang, C. Wan, Y. Zhang, Morphology and electrical properties of polyamide 6/polypropylene/multi-walled carbon nanotubes composites. Compos. Sci. Technol. 69 (2009) 2212–2217.

[21] L. Li, C. Miesch, P. Sudeep, A. C. Balazs, T. Emrick, T. P. Russell, R. C. Hayward, Kinetically trapped co-continuous polymer morphologies through intraphase gelation of nanoparticles, Nano Lett. 11 (2011) 1997-2003.

[22] H. J. Chung, K. Ohno, T. Fukuda, R. J. Composto, Self-regulated structures in nanocomposites by directed nanoparticle assembly, Nano Lett. 5 (2005) 1878-1882.
[23] L. Elias, F. Fenouillot, J.-C. Majesté, P. Cassagnau, Morphology and rheology of immiscible polymer blends filled with silica nanoparticles, Polymer 48 (2007) 6029-6040.
[24] B. Du, U. A. Handge, M. Wambach, C. Abetz, S. Rangou, V. Abetz, Functionalization of MWCNT with p(mma-co-s) copolymers via ATRP: influence on localization of MWCNT in SAN/PPE 40/60 blends and on rheological and dielectric properties of the composites, Polymer 54 (2013) 6165-6176.
[25] S. Bose, A. R. Bhattacharyya, P. V. Kodgire, A. Misra, Fractionated crystallization in PA6/ABS blends: Influence of a reactive compatibilizer and multiwall carbon nanotubes, Polymer 48 (2007) 356-362.
[26] J. Y. Feng, C. M. Chan, J. X. Li, A method to control the dispersion of carbon black in an immiscible polymer blend, Polym. Eng. Sci. 43 (2003) 1058–1063.
[27] A. L. Persson, H. Bertilsson, Viscosity difference as distributing factor in selective absorption of aluminium borate whiskers in immiscible polymer blends, Polymer 39 (1998) 5633–5642.
[29] J. J. Stickel, R. L. Powell, Fluid mechanics and rheology of dense suspensions. Annu. Rev. Fluid Mech. 37 (2005) 129–149.
[30] P. Van Puyvelde, A. Vananroye, R. Cardinaels, P. Moldenaers, Review on morphology development of immiscible blends in confined shear flow, Polymer 49 (2008) 5363–5372.
[31] Baudouin, A.C. Auhl D. Tao, F. Devaux J. Bailly, C. Polymer blend emulsion stabilization using carbon nanotubes interfacial . Polymer 2011, 52, 149–56.
[32] A. C. Baudouin, C. Bailly, J. Devaux, Interface localization of carbon nanotubes in blends of two copolymers, Polym. Degrad. Stab. 95 (2010) 389–398.
[33] Z. Xu, Y. Zhang, Z. Wang, N. Sun, H. Li, Enhancement of electrical conductivity by changing phase morphology for composites consisting of polylactide andpoly (ε-caprolactone) filled with acid-oxidized multiwalled carbon nanotubes, ACS Appl Mater Interfaces 3 (2011) 4858-4864.
[34] A. Bharati, R. Cardinaels, T. Van der Donck, J. W. Seo, M. Wübbenhorst, P. Moldenaers, Tuning the phase separated morphology and resulting electrical conductivity of carbon nanotube filled PaMSAN/PMMA blends by compatibilization with a random or block copolymer, Polymer 108 (2017) 483-492.
[35] A. Bharati, R. Cardinaels, J. W. Seo, M. Wübbenhorst, P. Moldenaers, Enhancing the conductivity of carbon nanotube filled blends by tuning their phase separated morphology with a copolymer Polymer 79 (2015) 271-282.
[36] C. McClory, P. Pötschke, T. McNally, Influence of screw speed on electrical and rheological percolation of melt-mixed high-impact polystyrene/MWCNT nanocomposites, Macromol. Mater. Eng., 296 (2011) 59–69.
[37] N. K. Shrivastava, S. Maiti, S. Suin, B. B. Khatua, Influence of selective dispersion of MWCNT on electricalpercolation of in-situ polymerized high-impact polystyrene/MWCNT nanocomposites, Express Polym Lett 8 (2014) 15–29.
[38] M. Klüppel, G. Heinrich, Fractal structures in carbon black reinforced rubbers. Rubber Chem. Technol. 68 (1995) 623-651.
[39] P.-G. De Gennes, On a relation between percolation theory and the elasticity of gels, J. Physique lett. 37 (1976) 1–2.
[40] J.-C. Majeste, F. Vincent, A kinetic model for silica-filled rubber reinforcement, J. Rheol. 59 (2015) 405–427.
[41] L. Moreira, R. Fulchiron, G. Seytre, P. Dubois, P. Cassagnau, Aggregation of Carbon Nanotubes in Semidilute Suspension, Macromolecules, 43 (2010) 1467–1472.
[42] I. Alig, P. Pötschke, D. Lellinger, T. Skipa, S. Pegel, G. R. Kasaliwal, T. Villmow, Establishment, morphology and properties of carbon nanotube networks in polymer melts, Polymer 53 (2012) 4–28.
[43] A. W. K. Ma, F. Chinesta, M. R. Mackley, The rheology and modeling of chemically treated carbon nanotubes suspensions J. Rheol. 53 (2009) 547–573.
[44] N. Jouault, P. Vallat, F. Dalmas, S. Said, J. Jestin, F. Boué, Well-dispersed fractal aggregates as filler in polymer-silica nanocomposites: long-range effects in rheology, Macromolecules, 42 (2009) 2031-2040.

[45] N. Jouault, F. Dalmas, F. Boué, J. Jestin, Multiscale characterization of filler dispersion and origins of mechanical reinforcement in model nanocomposites, Polymer 53 (2012) 761-765.
[46] M. Klüppel, R. Schuster, G. Heinrich, Structure and properties of reinforcing fractal filler networks in elastomers. Rubber Chem. Technol. 70 (1997) 243-255.
[47] G. Heinrich, M. Klüppel, The role of polymer-filler interphase in reinforcement of elastomers, Kaut. Gummi Kunstst. 57 (2004) 452-454.
[48] M. Klüppel, The role of disorder in filler reinforcement of elastomers on various length scales. Adv. Polym. Sci. 164 (2003) 1-86.
[49] P. Pötschke, L. Haeussler, S. Pegel, R. Steinberger, G. K. Scholz, Thermoplastic polyurethane filled with carbon nanotubes for electrical dissipative and conductive applications, Kaut. Gummi Kunstst. 60 (2007) 432–437.
[50] P. Pötschke, M. Abdel-Goad, I. Alig, S. Dudkin, D. Lellinger, Rheological and dielectrical characterization of melt mixed polycarbonate-multiwalled carbon nanotube composites, Polymer 45 (2004) 8863-8870.
[51] E. K. Hobbie, D. J. Fry, Nonequilibrium Phase Diagram of Sticky Nanotube Suspensions, Phys. Rev. Lett. 97 (2006) 036101.
[52] E. E. Ureña-Benavides, M. J. Kayatin, V. A. Davis, Dispersion and Rheology of Multiwalled Carbon Nanotubes in Unsaturated Polyester Resin, Macromolecules 46 (2013) 1642−1650.
[53] W. Li, S. T. Buschhorn, K. Schulte, W. Bauhofer, The imaging mechanism, imaging depth, and parameters influencing the visibility of carbon nanotubes in a polymer matrix using a SEM, Carbon 49 (2011) 1955-1964.
[54] W. Li, W. Bauhofer, Imaging of CNTs in a polymer matrix at low accelerating voltages using a SEM, Carbon 49 (2011) 3891-3898.
[55] R. B. Bird, R. C. Armstrong, O. Hassager, In Dynamics of polymeric liquids, Vol. 1, Fluid mechanics, 2nd Ed., John Wiley and Sons Inc., New York 1987 p 784.
[56] J. D. Ferry, In Viscoelastic properties of polymers, 3rd Ed., John Wiley and Sons Inc., New York 1980.
[57] M. L. Williams, R. F. Landel, J D. Ferry, The temperature dependence of relaxation mechanisms in amorphous polymers and other glass-forming liquids, J. Am. Chem. Soc. 77 (1955) 3701–3707
[58] M. Marcourt, P. Cassagnau, R. Fulchiron, D. Rousseaux, O. Lhost, S. Karam, An original combined method for electrical conductivity measurement of polymer composites under extensional deformation, J. Rheol. 61 (2017) 845-857.
[59] A. Barber, S. Cohen, H. Wagner, Static and dynamic wetting measurements of single carbon nanotubes, Phys. Rev. Lett. 92 (2004) 186103.
[60] Y. Sun, Z.-X Guo, J. Yu, Effect of ABS Rubber Content on the Localization of MWCNTs in PC/ABS Blends and Electrical Resistivity of the Composites. Macromol. Mater. Eng. 295 (2010) 263–268.
[61] S. Kirkpatrick, Percolation and conduction. Rev. Mod. Phys. 45 (1973) 574–588.
[62] W. Bauhofer, J. Z. Kovacs, A review and analysis of electrical percolation in carbon nanotube polymer composites. Compos. Sci. Technol. 69 (2009) 1486–1498.
[63] I. Balberg, N. Binenbaum, N. Wagner, Percolation thresholds in the 3-dimensional sticks system. Phys. Rev. Lett. 52 (1984) 1465–1468.
[64] S. S. Rahatekar, K. K. Koziol, S. R. Kline, E. K. Hobbie, J. W Gilman, A.H. Windle, Length-Dependent Mechanics of Carbon-Nanotube Networks, Adv. Mater. 21 (2009) 874–878.
[65] I. Alig, T. Skipa, D. Lellinger, P. Pötschke, Destruction and formation of a carbon nanotube network in polymer melts: Rheology and conductivity spectroscopy, Polymer 49 (2008) 3524-3532.
[66] W.-H. Shih, W. Y. Shih, S.-I. Kim, J. Liu, I. A. Aksay, Scaling behavior of the elastic properties of colloidal gels, Phys. Rev. A, 42 (1990) 4772−4779.
[67] F. Khalkhal, P. J. ,Carreau, Scaling behavior of the elastic properties of non-dilute MWCNT–epoxy suspensions, Rheol. Acta 50 (2011) 717−728.
[68] C. B. Weinberger, J. D. Goddard, Extensional flow behavior of polymer solutions and particle suspensions in a spinning motion, Int. J. Multiphase Flow, 1 (1974) 465-486.
[69] R. Krishnamoorti, J. Ren, A. Silva, Shear response of layered silicate nanocomposites, J. Chem. Phys. 114 (2001) 4968–4973.

[70] V. C. Barroso, S. P. Ribeiro, J. M. Maia, Unusual extensional behavior of a polystyrene/HIPS blend, Rheol. Acta 42 (2003) 483-490.
[71] I. Alig, D. Lellinger, S. M. Dudkin, P. Pötschke, Conductivity spectroscopy on melt processed polypropylene-multiwalled carbon nanotube composites: recovery after shear and crystallization, Polymer 48 (2007) 1020–1029.
[72] I. Alig, T. Skipa, M. Engel, D. Lellinger, S. Pegel, P. Pötschke, Electrical conductivity recovery in carbon nanotube polymer composites after transient shear, Phys. Status Solidi B 244 (2007) 4223–4226.
[73] I. Alig, D. Lellinger, M.Engel, T. Skipa, P. Pötschke, Destruction and formation of a conductive carbon nanotube network in polymer melts: in-line experiments, Polymer 49 (2008) 1902–1909.
[74] I. Alig, T. Skipa, D. Lellinger, M. Bierdel, H. Meyer, Dynamic percolation of carbon nanotube agglomerates in a polymer matrix: comparison of different model approaches, Phys. Status Solidi B 245 (2008) 2264–2267.
[75] I. Alig, T. Skipa, D. Lellinger, P. Pötschke, Destruction and formation of a carbon nanotube network in polymer melts: rheology and conductivity spectroscopy, Polymer 49 (2008) 3524–3532.

List of Figures and Tables

Figure 1: Master curve of PS (filled symbols) and HIPS (open symbols) matrices built for a reference temperature of 200°C. Symbols: Experimental data G' and G", Solid lines: Discrete Maxwell model.

Figure 2: TEM micrograph of HIPS filled with 0.82 vol% CNT.

Figure 3 SEM micrographs of PS filled with 0.79 vol% MWCNT (left) and HIPS filled with 0.82 vol% MWCNT (right), magnification = x2000, WD 5mm 20kV and in-lens detector.

Figure 4: Evolution of the conductivity as a function of the volume fraction of MWCNT. Empty circles and filled squares: raw data. Solid and dashed lines: percolation laws **respectively for the PS and HIPS matrices**. Filled circles: conductivity measured in the HIPS matrix and plotted versus the volume fraction of CNT in PS Phase (see Eq. 8).

Figure 5: Storage moduli versus angular frequency at 200°C for PS composites.

Figure 6: Storage moduli versus angular frequency at 200°C for HIPS composites (indicated volume concentrations are concentrations in the PS phase).

Figure 7: Variation of the equilibrium modulus as a function of the CNT volume fraction in PS continuous phase.

Figure 8: Ratio between extensional viscosity at 0.1 s^{-1} of the composites and the shear viscosity of the matrices at 180°C.

Figure 9: Conductivity evolution under extensional deformation at 180°C for an extensional rate of 0.01 s^{-1}.

Figure 10: SEM micrographs of the two composites after a Hencky deformation of 1 at 160°C and 0.01 s^{-1} a) PS filled with 0.79 vol% CNT, b) HIPS filled with 0.82 vol% CNT in the PS phase and the conductivity is around 8.10^{-5} $S.cm^{-1}$ for the two specimens. The scale bar is 2µm.

Figure 11: WLF plot for the a_T shift factor from the build of the master curve of the pure matrices and from the build of the master curve of conductivity recovery. The reference temperature (T_0) is 180°C.

Figure 12: Conductivity recovery under quiescent condition at 170°C of PS filled 0.79 vol% CNT and HIPS filled with 0.82 vol% CNT after a Hencky deformation of 1 at 170°C and 0.01 s^{-1}.

Figure 13: Conductivity variation for PS filled with 0.79 vol% CNT (a) and HIPS filled with 0.82 vol% CNT (b) under extensional conditions that lead to large and low W_i for the two composites.

Figure 14: Evolution of the Hencky strain value when the composites conductivity reaches 10^{-6} S/cm as a function of the filler volume fraction for the two types of matrix for specimen under extensional rate fixed at 0.1 s^{-1} at 160°C a) and at 180°C b).

Figure 15: Evolution of the Hencky strain value when the composites conductivity reaches 10^{-6} S/cm as a function of the filler volume fraction for the two types of matrix for specimen under extensional rate fixed at 0.1 s^{-1} at 200°C a) and at 210°C b).

Table 1: Shift factors a_T and weight average relaxation times for the two matrices calculated for different temperatures